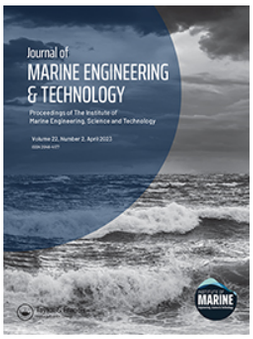

Taylor & Francis
Taylor & Francis Group

Journal of Marine Engineering & Technology

ISSN: (Print) (Online) Journal homepage: https://www.tandfonline.com/loi/tmar20

Filtering based multi-sensor data fusion algorithm for a reliable unmanned surface vehicle navigation

Wenwen Liu, Yuanchang Liu & Richard Bucknall

To cite this article: Wenwen Liu, Yuanchang Liu & Richard Bucknall (2023) Filtering based multi-sensor data fusion algorithm for a reliable unmanned surface vehicle navigation, Journal of Marine Engineering & Technology, 22:2, 67-83, DOI: 10.1080/20464177.2022.2031558

To link to this article: https://doi.org/10.1080/20464177.2022.2031558

Published online: 01 Feb 2022.

JOURNAL OF MARINE ENGINEERING & TECHNOLOGY
2023, VOL. 22, NO. 2, 67–83
https://doi.org/10.1080/20464177.2022.2031558

Filtering based multi-sensor data fusion algorithm for a reliable unmanned surface vehicle navigation

Wenwen Liu, Yuanchang Liu and Richard Bucknall

Department of Mechanical Engineering, University College London, London, UK

ABSTRACT

When considering the working conditions under which an unmanned surface vehicle (USV) operates, the navigational sensors, which already have inherent uncertainties, are subjected to environment influences that can affect the accuracy, security and reliability of USV navigation. To combat this, multi-sensor data fusion algorithms will be developed in this paper to deal with the raw sensor measurements from three kinds of commonly used sensors and calculate improved navigational data for USV operation in a practical environment. Unscented Kalman Filter, as an advanced filtering technology dedicated to dealing with non-linear systems, has been adopted as the underlying algorithm with the performance validated within various computer-based simulations where practical, dynamic navigational influences, such as ocean currents, provide force against the vessel's structure, are to be considered.

ARTICLE HISTORY
Received 29 April 2021
Accepted 14 January 2022

1. Introduction

Development of autonomous vehicle control is advancing rapidly within the maritime industry. Unmanned Surface Vehicles (USV)s can provide benefits to both civilian applications and military operations. Increased interest in further development of USVs has been witnessed worldwide, driven by their capabilities to perform a large range of missions. A number of remotely controlled USVs have been constructed and are in service, such as the CEE-USV developed by CEE HydroSystems which is used to conduct mine tailings and bathymetry surveys in Arizona, USA (CEE HydroSystems 2017). Autonomous marine navigation is needed for new commercial and civilian vessels. China has developed and unmanned cargo ship Jin Dou Yun 0 Hao which has completed several test voyages since 2019 with subsequent order for the first autonomous container ship and plans to build a fleet of unmanned cargo ships (Wang et al. 2020). In Europe an EU project AEGIS (Advanced Efficient and Green Intermodal Services) aims is developing a system that autonomous surface vessels to operate with autonomous port authorities (Rødseth et al. 2020). Naval interest in USVs has increased too in recent years, such as the Royal Navy's interest in the maritime demonstrator 'Madfox' designed to test and develop new technologies for the purposes of undertaking a wide range of army operations including surveillance and protection (Casola et al. 2018). The US Navy has a developing Large Unmanned Surface Vessel as a potential replacement for its large capacity warships (Costa et al. 2019).

In the meantime, the research into USVs for autonomous operations is undergoing active development and a key challenge resides in developing autonomous navigation systems for such applications. Note that with the rapid development of marine electronic navigation technology, especially the Global Positioning System (GPS), improving the viability of the USVs is attracting increasing attention from academic and commercial companies, driven by their capability to undertake various maritime missions, which are listed in Table 1.

Table 1. Various examples of missions that USVs can accomplish.

Commercial missions	Military missions
Marine monitoring	Anti-terrorism forces
Marine waste detection	Protection forces
Mapping the marine funds and mining	Electronic warfare
Shipping	Mine Countermeasure
Cooperate with UUVs and UAVs	Anti-submarine warfare
Sea surveillance	Post explosion assessment
Environmental monitoring	Threat identification and classification
Water sampling	Harbour patrol

In order to complete a mission, all autonomous USVs must have positional certainty of location, be situationally aware in relation to the surrounding environment, as well as other dedicated abilities, for the specific tasks such as speed and directional control, path planning ability and obstacle and hazard avoidance. If human remote control were to be reduced and/or eliminated, certain missions would require a high degree of autonomy within the USV's functionality, therefore, researchers are keen to improve USV autonomy. According to Liu et al. (2016), USV development is focused on four main aspects (Table 2): USV hull and auxiliary structural elements; propulsion and power systems; Navigation, Guidance and Control (NGC) system; communication system and ground station. In order to increase USVs' level of autonomy, improvement in the NGC system is core to that development. Navigation systems of this type and functionality should have the ability to accurately determine the location of the USV itself as well as perceiving the surrounding environment so that safe paths of operation can be generated along which the USV would then transit.

As shown in Figure 1, an autonomous navigation system, also referred to as the Navigation Guidance and Control (NGC) system, is composed of three modules: a data acquisition module (Navigation), a path planning module (Guidance), and an advanced control module (Control). First, the data acquisition module acquires

CONTACT Yuanchang Liu yuanchang.liu@ucl.ac.uk Department of Mechanical Engineering, University College London, Torrington Place, London WC1E 7JE, UK

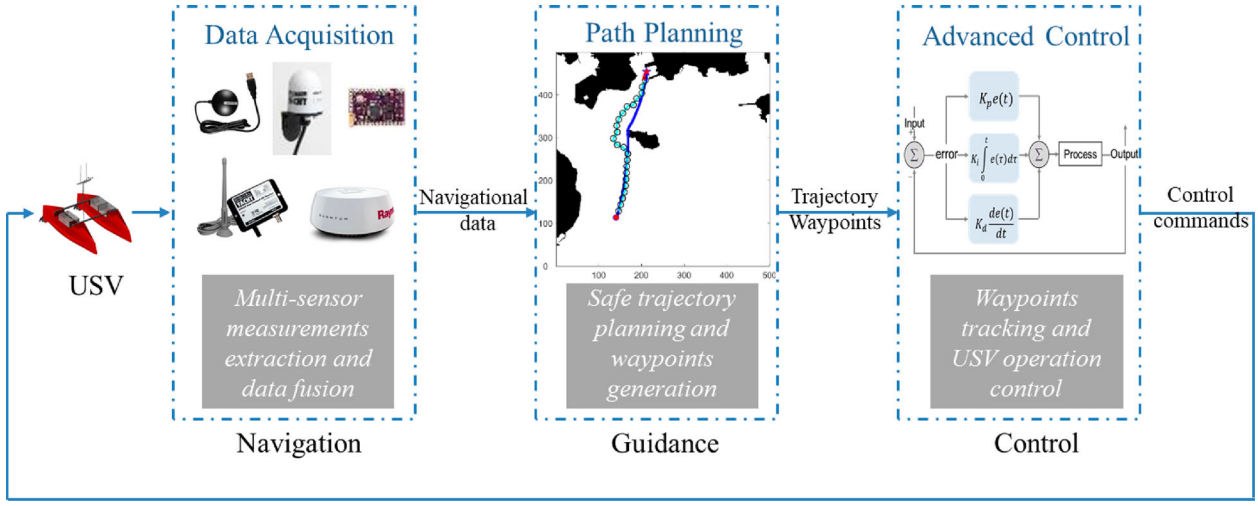

Figure 1. Autonomous navigation system (NGC system) of an unmanned surface vehicle.

Table 2. Four main research sectors and main research results of USVs.

Research sectors	Main research results
USV hull and auxiliary structural elements	• Kayaks hull structure (Curcio et al. 2005) • Catamarans hull structure (Naeem et al. 2008) • Trimarans hull structure (Peng et al. 2009) • Wave resistant hull structure (Guan et al. 2021)
Propulsion and power systems	• Water-jet powered USV (Han et al. 2017) • High-speed diesel-electric hybrid USV (Zhuang et al. 2021) • Renewable energy powered USV (Zhou et al. 2015)
Navigation, Guidance and Control	• Computer-vision based environment perception (Chen et al. 2021) • Motion planning and decision-making (Wang et al. 2021) • Automatic control (Zhou et al. 2019) • Validation and verification (Haseltalab et al. 2020) • Docking control (Li et al. 2020)
Communication system and ground station	• USVs based future maritime communication networks (Yang et al. 2019) • Underwater communication based on USVs (Lv et al. 2021)

information pertaining to the USV's own position, speed and heading (obtained using various navigation sensor). It also constructs the surrounding operational environment by detecting target ships (TSs). Based on this information, the path planning module is then tasked to generate a safe path, usually defined by a series of waypoints, along which the USV will navigate. Finally, the advanced control module uses the generated waypoints, which may be either predetermined as part of a mission or generated by the path planning algorithm, as reference points to guide the USV, to ensure that the USV adheres to the generated path by controlling its propulsion and steering system.

While at sea, accurate measurements of position, speed, and heading are vital to ensure a vessel reaches its destination safely. The need for accurate positional information is critical once the vessel is on passage. Other vessel traffic and waterway hazards can increase the complexity of the manoeuvring that may be required and the risk of accidents (National Coordination Office 2014). Therefore, the data acquisition module responsible for obtaining and processing real time navigational data constitutes the fundamental component of an autonomous navigation system. This research focuses on the navigation and guidance function of USV operation, with particular focus on improvements in reliability and resilience of the navigation function through use of data fusion methodologies that can be applied to disparate navigation sensor and data gathering technologies.

It will be through the reinforcement of such technologies that the author will seek to provide novel solutions to the problems that can affect the security and reliability of transit for autonomous USVs caused by failings to which standard navigation devices are prone. This work supports and complements work on path planning and fleet orientation of USVs that has been carried out by other colleagues in the marine research group of UCL. Typical works include the investigation on multi-USV planning and coordination (Zhou et al. 2019), machine-learning powered automatic control (Wang et al. 2021) and multi-task allocation for multi-agent systems in ocean environments (Ma et al. 2021). Together with these works, the success of the work in this paper, where sensing and perception technologies have been well addressed, can well complete an autonomous navigation system and provide critical control/guidance commends for USVs when navigating in challenging maritime environments.

Contemporarily, the most widely used navigation method is the Global Navigation Satellite System (GNSS), which can provide absolute positional information in open areas. However, the GNSS can suffer from problems of signal reliability and continuity under harsh environmental conditions. If the GNSS were to fail, then the consequences for an autonomous USV could be disastrous. The ship would have limited certainty as to its current position and other navigational instruments working off the data provided may have their functionality degraded. Therefore, instead of relying solely on the satellite navigation system, the recent trend is to acquire continuous and acceptably precise navigational data by interfacing a dead-reckoning (DR) system and using multi-sensor data fusion (MSDF) techniques (Appriou 2014).

It also should be noted that the operating conditions of USVs are often hazardous and unpredictable. Therefore, accurate and reliable navigational data is a primary demand to ensure the safety of the USV. Integrated navigation systems that comprise multiple sensors are normally employed to provide more accurate, continuous and reliable navigational data (Allerton and Jia 2005; Stateczny and Kazimierski 2011; Groves 2013; Paulino et al. 2019). This has many advantages, such as improving system reliability and robustness, extending measurement coverage, increasing data confidence and improving resolution (Xie and Wan 2011). Through the use of multiple sensors, the system could gather a large amount of navigational data. If this is an outcome, then the optimal estimation

techniques applied to fuse the data obtained will reside at the core of a multi-sensor navigation system.

It should be noted that an accurate estimation of USVs navigational data is critical to ensure a safe navigation for USVs, which includes facilitating path planning algorithms calculating collision free trajectories and controllers generating reliable control commands. Such a motivation is inspired by the authors' previous field trials on a practical USV, *Springer* USV, at Roadford Lake, UK. During the tests, an optimised trajectory was generated using an improved A∗ algorithm and a PID control was implemented on the *Springer* to track waypoints and follow the trajectory. From the results, it has been found that even a fine-tuned PID controller could not ensure a perfect tracking performance, i.e. a deviation was always generated between the actual path taken by the *Springer* and the planned trajectory due to various environmental influences. Without a good estimation of a vessel's state (position or velocity), such a deviation could be well reduced, which will seriously affect the controller's performance.

This paper therefore proposes a reliable multi-sensor data fusion algorithm based upon unscented Kalman filter (KF) technology to properly address the reliable navigation problem for USVs. The proposed algorithm is able to deal with the raw sensor measurements from three types of sensors (inertial measurement unit (IMU), GPS and electronic compass) and calculate improved navigational data for USV operation in a practical environment. The algorithm presented in this paper is an upgraded work to a previous publication at INEC 2020 (Liu et al. 2020), which provides a detailed discussion on the future navigational technologies for USVs. In that paper, KF based fusion technologies have been reviewed and designed but without full consideration of the non-linear dynamic characteristics of USVs' motion. This paper therefore elevates the work in (Liu et al. 2020) by first proposing a full non-linear dynamic model of the USV. Next, an unscented Kalman filter (UKF) algorithm, which is specialised in providing estimation for non-linear systems, is used as the underlying filtering algorithm for multi-sensor data fusion. Intensive simulations with different USV motion models have been carried out to validate the effectiveness of the proposed algorithms.

2. Literature review

The Kalman Filter (KF), a linear recursive data processing algorithm, is extensively used in vehicle navigation. It processes all available attributes, regardless of their precision, to estimate the current value of the variables of interest, using knowledge of the system and measurement device dynamics; the statistical description of the system noise, measurement errors, and uncertainty in the dynamic models; as well as available information regarding initial conditions of the variables of interest (Maybeck 1979; Choi et al. 2020; Han et al. 2021). If the input data fits the predefined linear dynamics and statistical models and *a priori* knowledge is known, the KF can provide an optimal estimate of the state vector, in a minimum variance sense (Gelb 1974). As a result, the KF has become the most common technique for estimating the state of a linear system, particularly in navigation systems. Rodriguez and Gomez (2009) developed three sensor fusion algorithms based on Kalman Filtering to locate an agricultural land vehicle by trying different combinations of existing navigation sensors. The first KF algorithm takes measurements from a GPS module and a steering angle sensor and outputs fused navigational data, i.e. position, heading and speed of the vehicle. The second KF algorithm they developed was used to provide corrections to GPS measurements from an electronic compass. They integrated an IMU with a GPS system with an extra steering angle sensor in the final algorithm for system linearisation. They concluded that combining a complementary sensor is an effective way to improve GPS signals.

However, a practical application of a KF to a specific problem requires correct configuration of its parameters. Li et al. (2015) used the KF to process the measurements from a conventional strap-down inertial navigation system to track a vehicle's attitude. They applied the developed algorithm to a practical vehicle with a rocking base and the repeated alignment achieved a precision of 0.04° over 180 s. Most of the other approaches using conventional KFs in navigation that can be found in published sources only deal with sensor sample integration in linear systems, or pre-processes the sensor signals to linearise the integrated system (Baselga et al. 2009; Xie and Wan 2011; Maklouf et al. 2013).

In practice, most systems are non-linear and the KF is incapable of making estimations with sufficient accuracy. Therefore, variant KFs have been developed to accommodate non-linear applications in the real world. Bijker and Steyn (2008) designed an IMU/GPS integrated system with two minor extended Kalman Filters (EKFs) to determine an unmanned airship's navigational data, i.e. attitude, velocity and position. They found that using one major EKF with all the navigational data as inputs generates more accurate estimations but requires more processing power. The trade-off between the accuracy and processing power has been mitigated by splitting the single EKF into two minor EKFs, namely the attitude estimator and position estimator. Saderzadeh (2010) proposed an EKF algorithm to handle the navigation error of a mobile robot. It was demonstrated that estimation at the primary state would introduce error into the system and the convergence rate of the EKF algorithm is low. Mousazadeh et al. (2018) used the EKF to estimate an USV's state and position. Although the authors did not provide the computational time of the EKF based algorithm, it necessitates the computation of a complex Jacobian matrix at each time step, hindering its adaptation to real time applications. Zhang et al. (2005) implemented an Unscented Kalman Filter (UKF) to improve the GPS, the IMU and the electronic compass measurements. The authors implemented both UKF and EKF and tested them in a practical land vehicle. The results showed that a UKF is able to produce estimated navigational data with greater accuracy than those generated by an EKF. The superior performance of a UKF over an EKF was further proved by Zhai et al. (2014) for GPS/INS integrated navigation, Choi et al. (2010) for on-board orbit determination using GPS observations, Lee et al. (2017) for nanosat attitude estimation and Gao et al. (2018) for INS/GNSS/CNS integration. Another interesting work was undertaken by Marchel et al. (2020), where an EKF has been integrated for a simultaneous location and mapping (SLAM) problem using range and bearing information. The proposed method was used to calculate an optimised position of navigational aids such that moving vessels can be better guided when navigating in a congested area.

Another variant of KF used for unmanned vehicle navigation was proposed by Motwani et al. (2013). They developed an Interval Kalman Filter (IKF) based algorithm to estimate the yaw dynamics of an uninhabited surface vehicle called *Springer* during operation. The system to determine *Springer's* yaw dynamic is linear, but the authors improved the conventional KF by adding the boundaries of system uncertainties to the algorithm using interval system models (Motwani et al. 2013). In recent years, a growing interest in developing mathematical techniques to deal with the impracticality of the conventional KF and its variants, such as fuzzy logic, adaptive estimations (Gao et al. 2012; Li et al. 2015; Meng et al. 2016; Motwani et al. 2016; Liu et al. 2019) has been witnessed.

A comparison of different KF technologies is summarised in Table 3. Most of the current research in USV navigation focuses on using variant filtering techniques to fuse raw sensor measurements without considering practical uncertainties associated with the sensors themselves within varied environments (Ccolque-Churquipa et al. 2018; Mousazadeh et al. 2018; Wang et al. 2018). There is

Table 3. Comparison of current sensor data fusion algorithms.

Sensor fusion algorithms	Feature
Kalman Filter (Kalman 1960)	Used in linear system
Extended Kalman Filter (Kalman and Bucy 1961)	Linearise the non-linear system using Taylor expansion
Unscented Kalman Filter (Julier and Uhlmann 1997)	Generates several Sigma points and propagate them through the non-linear state function directly
Interval Kalman Filter (Chen et al. 1997)	Add boundaries to system uncertainty

a knowledge gap in developing a practical autonomous navigation system to address the above practical problems in real-life USV developments.

3. Nonlinear USV navigation model and system measurement model

3.1. Nonlinear USV motion model

The working condition of an intelligent USV operation is time-varying. The state of an autonomous navigation system incorporates the USV's navigational data, i.e. position (p), velocity (v) and heading (θ), which are governed by a discrete time state-space model of the USV dynamic system in a two-dimensional navigation frame. Instead of fully relying on the system model, the acceleration rate (a) and rotation rate (ω), which can be measured by inertial sensors, are used to compute each of the models of navigational data using discrete integration. The integration of the inertial measurements brings a more accurate ship motion model that can then be expressed as:

$$\boldsymbol{p}(k) = \boldsymbol{p}(k-1) + T \times \boldsymbol{v}(k-1) + \frac{1}{2}T^2 \times \boldsymbol{a}(k-1) \quad (1)$$

$$\boldsymbol{v}(k) = \boldsymbol{v}(k-1) + T \times \boldsymbol{a}(k-1) \quad (2)$$

$$\theta(k) = \theta(k-1) + T \times \omega(k) \quad (3)$$

where T is the processing time between two consecutive sampling steps.

Equations (1) to (3) can be viewed as the transition state models with p, v and θ being the state of the system, which are the estimation objects of the Kalman filter. Therefore, the state vector $\boldsymbol{x}$ with required data can be defined as:

$$\boldsymbol{x} = [p_x \;\; p_y \;\; v_x \;\; v_y \;\; \theta]^T \quad (4)$$

where p_x and p_y represent the positions in a north-east navigation frame, v_x and v_y are velocities and θ is the heading of the USV.

From the start of USV operation, the on-board IMU starts to measure the motions of the USV, that is, the accelerometer measures the accelerations and the gyroscope measures the angular velocity of the USV. Normally, acceleration rates provided by the IMU are along the inertial frame, which can be approximated as the body frame; whereas, other navigation information has been presented in the navigation frame. It therefore should convert the IMU data from the inertial frame to the navigation frame by using the rotation matrix:

$$\begin{bmatrix} a_{nx} \\ a_{ny} \end{bmatrix} = \begin{bmatrix} cos\emptyset & -sin\emptyset \\ sin\emptyset & cos\emptyset \end{bmatrix} \begin{bmatrix} a_{ix} \\ a_{iy} \end{bmatrix} \quad (5)$$

As shown in Figure 2, the heading that can be obtained from the compass is the clockwise angle referenced to North. Therefore, the anti-clockwise rotation angle from inertial frame (i-frame) to navigation frame (n-frame) is equal to the heading:

$$\begin{bmatrix} a_{nx}(k) \\ a_{ny}(k) \end{bmatrix} = \begin{bmatrix} cos\theta(k) & -sin\theta(k) \\ sin\theta(k) & cos\theta(k) \end{bmatrix} \begin{bmatrix} a_{ix}(k) \\ a_{iy}(k) \end{bmatrix} \quad (6)$$

It can be observed that the conversion of the frames generates the non-linearity of the system. Unscented Kalman filtering, uses an unscented transform to propagate designed Sigma points and calculates the mean of the propagated point to compute the optimal estimation of the input data. It has been used increasingly in vehicle navigation in recent years (Ma et al. 2014; Meng et al. 2016). As stated previously, when the frame rotation angle is equal to the heading of the USV, the non-linear dynamic model can then be obtained by combining Equation (6) and Equations (1) to (3) as

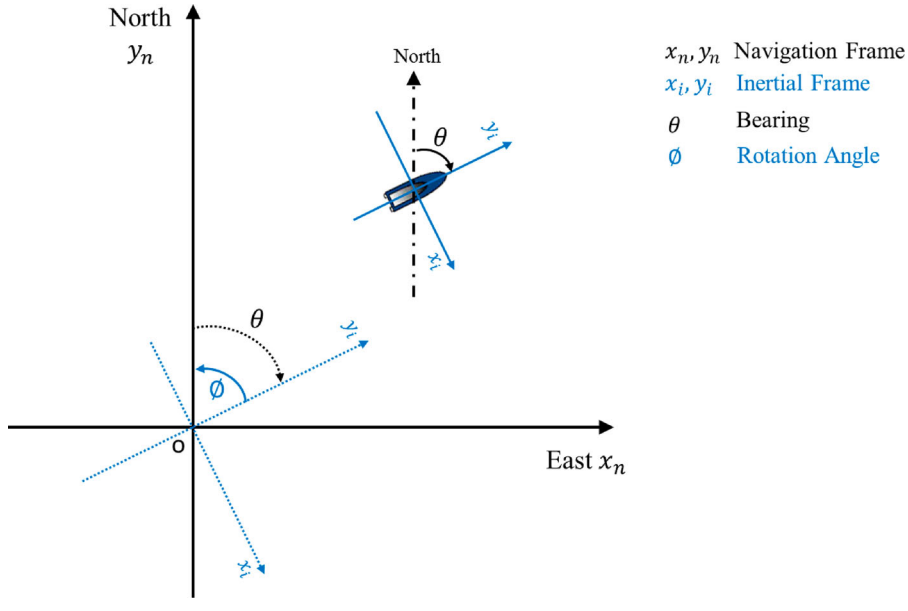

Figure 2. Conversion from i-frame to n-frame.

below:

$$f'(x) = \begin{pmatrix} \dot{p}_x \\ \dot{p}_y \\ \dot{v}_x \\ \dot{v}_y \\ \dot{\psi} \end{pmatrix} = \begin{pmatrix} v_x \\ v_y \\ cos\psi\, a_{ix} - sin\psi\, a_{iy} \\ sin\psi\, a_{ix} + cos\psi\, a_{iy} \\ \omega \end{pmatrix} \quad (7)$$

3.2. System measurement model

A GNC system obtains the absolute observations (measurements) of the USV's position and heading from a GPS sensor and an electronic magnetic compass. The absolute measurements are associated with random noises, which are described as Rooted Mean Square (RMS) errors in the sensor manuals. RMS error indicates that at 68% probability that the measurement lies within the range of the error from the true position and twice the range at 95% probability. Therefore, the sensor models of GPS can be defined with an additive noise component as:

$$p_o = p_i + v_g \quad (8)$$

The major magnetic measurement error results from the distortion of the Earth's magnetic field by nearby ferrous effects, sensor noise and magnetic interference. In practical applications, compasses are mounted in vehicles and platforms that usually have ferrous materials nearby. These nearby ferrous materials will generate permanent magnetic fields (hard irons) or varying magnetic fields (soft irons) to distort the Earth's magnetic field. Soft irons affect the magnetometer output by varying amounts depending on the compass orientation. This varying bias effect will distort the shape of the 2D magnetic field locus from a circle into an ellipse. Hard and soft iron distortions are the major error sources for magnetic compasses and compensating for these effects is essential to their application (Langley 2003). Normally, a calibration process is conducted to remove the bias after installation since the bias is constant without change of installation environment. In a similar manner to the GPS module, the electronic compass also provides absolute measurements of vehicle's headings with an additive random noise that can be expressed as Equation (9).

$$\theta_o = \theta_i + v_h \quad (9)$$

where p_i and θ_i are the true position and heading respectively; p_o and θ_o are the noisy measurements; and v_g and v_h are the uncertainty with a normal distribution with the standard deviation of their RMS error value r_g and r_h.

Therefore, the measurement model z can be denoted as:

$$\boldsymbol{z}(k) = \begin{bmatrix} p(k) \\ \theta(k) \end{bmatrix} + \begin{bmatrix} v_g(k) \\ v_h(k) \end{bmatrix}. \quad (10)$$

Based upon the observation equation in KF, the complete measurement equation can be rewritten as:

$$\boldsymbol{z}(k) = \begin{bmatrix} 1 & 0 & 0 & 0 & 0 & 0 \\ 0 & 1 & 0 & 0 & 0 & 0 \\ 0 & 0 & 0 & 0 & 0 & 1 \end{bmatrix} \begin{bmatrix} p_x(k) \\ p_y(k) \\ v_x(k) \\ v_y(k) \\ \theta(k) \end{bmatrix} + \boldsymbol{v}(k) \quad (11)$$

where $\boldsymbol{v}$ represents additive system measurement noise, which is also assumed to be white noise with zero mean and standard deviations given by r_g and r_h.

R, the covariance of measurement noise v is then given by:

$$\boldsymbol{R} = cov(\boldsymbol{v}) = \begin{bmatrix} {r_g}^2 & 0 & 0 \\ 0 & {r_g}^2 & 0 \\ 0 & 0 & {r_h}^2 \end{bmatrix} \quad (12)$$

The marine environment is uncertain and complex for USV navigation. There are various aspects that could cause position offset, especially environmental influences. Tidal current, wind and wave impacts are the most significant effects that would cause drift and deviation from course of a vessel moving on the water surface. In this context, the trajectory of an USV is complex and cannot be characterised simply as operating along a straight line or a curve of fixed radius in practice. If using a conventional Kalman Filter, the system has to be linear, and in the previous section the non-linearity caused by the frame conversion was neglected by assuming that only minimal heading change will occur during each time step. However, such an approximation may lead to large errors in practical applications, especially when the USV is not following a straight line. Thus, Kalman Filter variants such as the Extended KF (EKF) and the Unscented KF (UKF) have been developed and used to deal with non-linear systems. It is for this reason that an UKF based multi-sensor data fusion algorithm has been developed in this paper to deal with issues that might occur in real world practical conditions when estimating the navigational data of the USV.

4. Unscented Kalman filter

Based on the measurements, the observation model has the same linear equation as Equation (11). For an n dimensional random variable $\boldsymbol{x}$ with mean $\boldsymbol{m}$ and covariance $\boldsymbol{P}$, the UKF employs the unscented transformation to form a set of 2n+1 weighted points, which are also called Sigma points. The working procedures of the UKF are also composed of the prediction and estimation steps as the conventional KF. In the autonomous navigation system with the above dynamic model and measurement model, the mean and covariance of the required navigational data are computed using the following steps:

Step 1: Form 2n+1 sigma points around the $\boldsymbol{x}$ at the last state ($n = 5$ where the dimension of state vector $\boldsymbol{x}$ is 5) using Equations (13) to (15):

$$\boldsymbol{\chi}_0(k-1) = \boldsymbol{m}(k-1) \quad (13)$$

$$\boldsymbol{\chi}_{\boldsymbol{i}}(k-1) = \boldsymbol{m}(k-1) + \sqrt{n+\lambda}\left[\sqrt{\boldsymbol{P}_{\boldsymbol{i}}(k-1)}\right] \quad (14)$$

$$\boldsymbol{\chi}_{\boldsymbol{i+n}}(k-1) = \boldsymbol{m}(k-1) - \sqrt{n+\lambda}\left[\sqrt{\boldsymbol{P}_{\boldsymbol{i}}(k-1)}\right], \quad i = 1, \ldots, n \quad (15)$$

The constant weights W_i^m and W_i^c that are associated to each sigma point are computed as follows:

$$W_0^m = \lambda/(n+\lambda) \quad (16)$$

$$W_0^c = \frac{\lambda}{(n+\lambda)} + (1 - \alpha^2 + \beta) \quad (17)$$

$$W_i^m = W_i^c = 1/2(n+\lambda), \quad i = 1, \ldots, 2n \quad (18)$$

where $\lambda = \alpha^2(n+\kappa) - n$. The parameters α and κ determine the spread of the sigma points around the mean. β describes the distributed information, of which the optimal value is 2 for Gaussian distribution.

Step 2: Propagate the calculated sigma points through the dynamic model

$$\hat{\boldsymbol{\chi}}_{\boldsymbol{i}}(k) = f(\boldsymbol{\chi}_{\boldsymbol{i}}(k-1)), \quad i = 0, \ldots, 2n \quad (19)$$

Step 3: Compute the predicted mean $\boldsymbol{m}^-(k)$ and the predicted covariance $\boldsymbol{P}^-(k)$ by multiplying each weight to the associated Sigma

point as following:

$$\boldsymbol{m}^{-}(k) = \sum_{i=0}^{2N} W_i^m \hat{\boldsymbol{\chi}}_i(k) \tag{20}$$

$$\boldsymbol{P}^{-}(k) = \sum_{i=0}^{2N} W_i^c (\hat{\boldsymbol{\chi}}_i(k) - \boldsymbol{m}^{-}(k))(\hat{\boldsymbol{\chi}}_i(k) - \boldsymbol{m}^{-}(k))^T + \mathbf{Q}(k-1) \tag{21}$$

where N is the dimension of the expended state space, which equals to $N_x + N_w + N_{\boldsymbol{v}}$. N_x is the dimension of the original state that equals to n; N_w and $N_{\boldsymbol{v}}$ are the dimensions of the white noise $\boldsymbol{w}$ and $\boldsymbol{v}$.

Step 4: For a linear observation model, sigma points are not required at the correction stage that results in reduced computational cost and higher accuracies. The Kalman Filter gain to correct the prior belief by reducing the mean square error is computed by Equations (22) and (23):

$$\boldsymbol{K}(k) = \boldsymbol{P}^{-}(k)\boldsymbol{H}^T \boldsymbol{S}(k)^{-1} \tag{22}$$

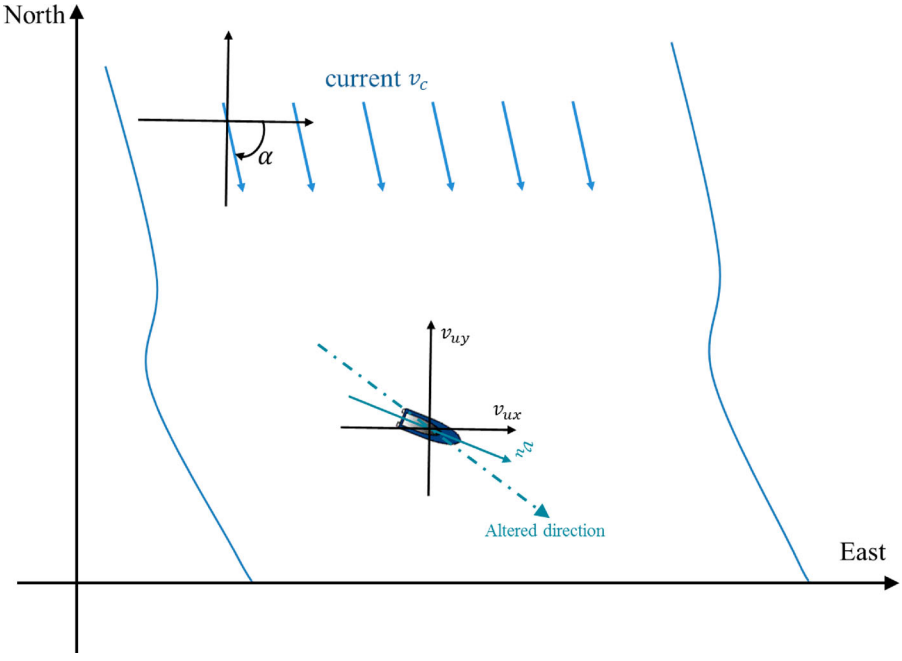

Figure 3. Calculation of Tidal effect to the USV speed.

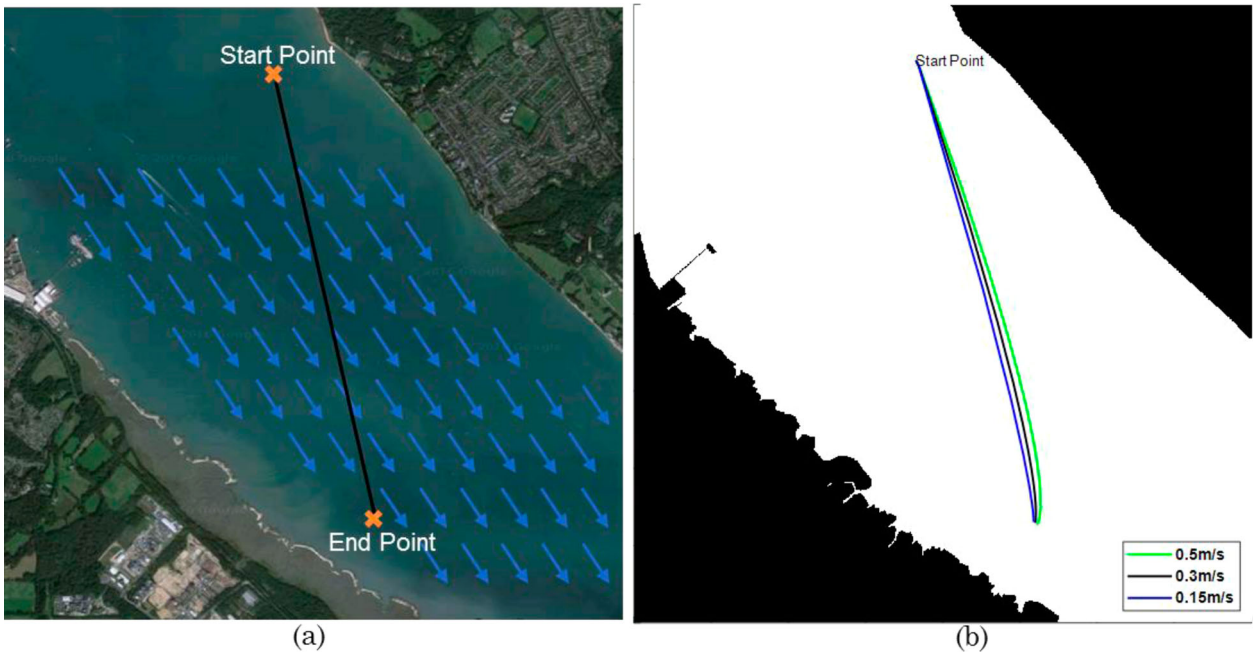

Figure 4. Simulation scenario 1: testing environment in Southampton east Cowes. (a) shows the satellite map with planed line trajectory of the USV, a constant current is also simulated along the water flow; (b) gives the binary map that converted from the satellite map with the drifted trajectory of the USV caused by three different currents.

$$\boldsymbol{S}(k) = \boldsymbol{H}\boldsymbol{P}^{-}(k)\boldsymbol{H}^{T} + \boldsymbol{R} \tag{23}$$

The optimal estimations $\hat{\boldsymbol{x}}(k)$ and $\boldsymbol{P}(k)$ of the navigation system given observation $\boldsymbol{z}(k)$ are updated by applying the Kalman Filter gain as shown in Equations (24) and (25).

$$\hat{\boldsymbol{x}}(k) = \hat{\boldsymbol{x}}^{-}(k) + \boldsymbol{K}(k)[\boldsymbol{z}(k) - \boldsymbol{H}\hat{\boldsymbol{x}}^{-}(k)] \tag{24}$$

$$\boldsymbol{P}(k) = (I - \boldsymbol{K}(k)\boldsymbol{H})\boldsymbol{P}^{-}(k) \tag{25}$$

5. Simulations of an UKF based multi-sensor data fusion algorithm

In order to simulate a USV operation in a practical environment, waypoint tracking missions have been simulated according to the map of the environment. The simulated USV calculates its distance and bearing to the next waypoint from the start. Once it researches proximity to the predesigned waypoint, which is termed waypoint clearance, it then searches for the next waypoint and steers to it until it reaches the final destination. The condition for a waypoint clearance is:

$$|p_{USV} - p_{wp}| = \sqrt{(p_{xUSV} - p_{xwp})^2 + (p_{yUSV} - p_{ywp})^2} < d \tag{26}$$

where $p_{USV} = (p_{xUSV}, p_{yUSV})$ is the current position of the USV, $p_{wp} = (p_{xwp}, p_{ywp})$ is the position of the target waypoint, d is the predesigned minimum radius around the waypoint. The USV can be considered as having reached the waypoint by entering the circle of radius d around the waypoint.

According to the waypoint clearance condition, the operation of the USV is adjusted by changing its headings to track the target waypoint as follows:

if $heading - bearing < \omega * T$, then the USV turns clockwise at the angular velocity ω, $heading = heading + \omega * T$;
if $heading - bearing > \omega * T$, then the USV turns anti-clockwise at the angular velocity ω, $heading = heading - \omega * T$;
if $heading - bearing = \omega * T$, then the USV remains its current direction, $heading = heading$,

Where ω is the angular velocity of the USV and T is the sampling time of the system. In this paper, the sampling time of the system is 1 s that is the same as the sampling rate of a typical GPS module. Accordingly, the sampling rate of the electronic compass has also been chosen at 1 s. The IMU normally provides measurement at a higher rate, for example 0.02 s, and an average of its sampled value in 1 s has been employed in the system.

The proposed algorithm has been implemented and verified using Matlab simulations during development. Measurements obtained from different navigational sensors including a GPS, an electronic compass and an IMU have been simulated by adding noises to the true values. For the GPS and the electronic compass, the readings are defined as the true value plus a white, normally distributed random measurement, noise with specific variance, which are normally provided in the sensor's manual. For the inertial measurements of the IMU, there will be an additional constant bias due to the magnetic field interference to the MEMS chips, and it can be predicted by suitable calibration. In a practical environment, sensor measurements accuracies could degrade. In this section, the simulated sensor noise settings may be larger than those in the sensor manuals and differ to the UKF predefined noise models that are based on the manuals. The sensor noise

Table 4. predefined sensor noises for simulations in practical environment.

		Noise	
Sensor	Measurement	Bias	Variance
IMU	Acceleration a_x	0.03 m/s^2	0.004 m/s^2
	Acceleration a_y	0.02 m/s^2	0.004 m/s^2
	Rotation rate ω	0.28°/s	0.033°/s
GPS	Position p_x	0	8 m
	Position p_y	0	7 m
Electronic Compass	Heading ψ	0	1°

Table 5. Simulation scenario 1: mean square errors.

Method	MSE 0.5 m/s	MSE 0.3 m/s	MSE 0.15 m/s	Units
UKF_position $\boldsymbol{p_x}$	4.972	4.746	3.8618	m^2
UKF_position $\boldsymbol{p_y}$	4.4747	4.2782	3.7013	m^2
GPS position $\boldsymbol{p_{gpsx}}$	66.6812	56.5433	63.4131	m^2
GPS position $\boldsymbol{p_{gpsx}}$	51.0834	48.0087	48.4819	m^2
UKF_heading $\boldsymbol{\psi}$	0.1109	0.0926	0.0892	deg^2
Electronic Compass $\boldsymbol{\psi_c}$	0.9261	0.9469	1.0015	deg^2

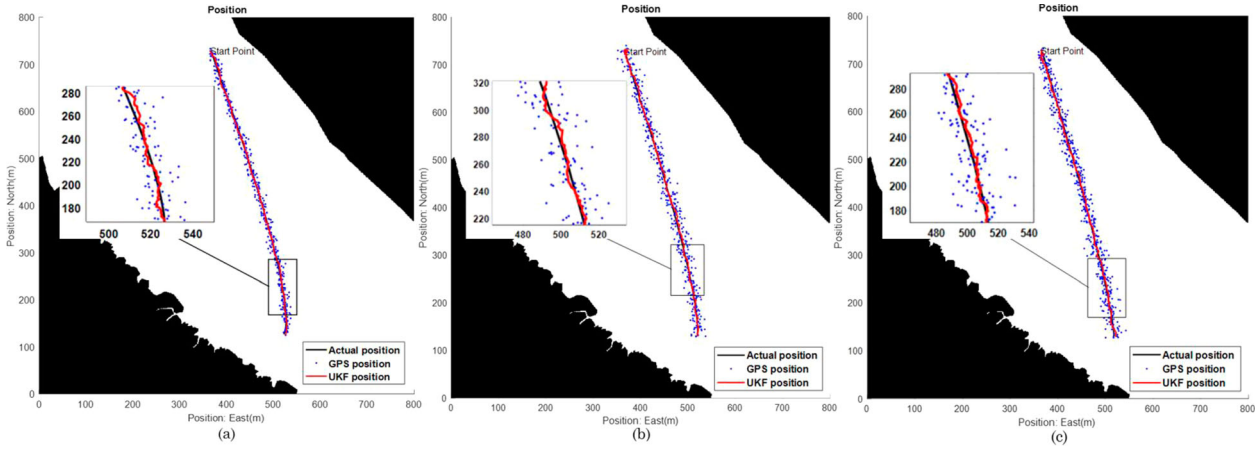

Figure 5. Simulation scenario 1: the converted binary map with the simulated GPS measurements and fused position results: (a) current: 0.5 m/s; (b) current: 0.3 m/s; (c) current: 0.15 m/s.

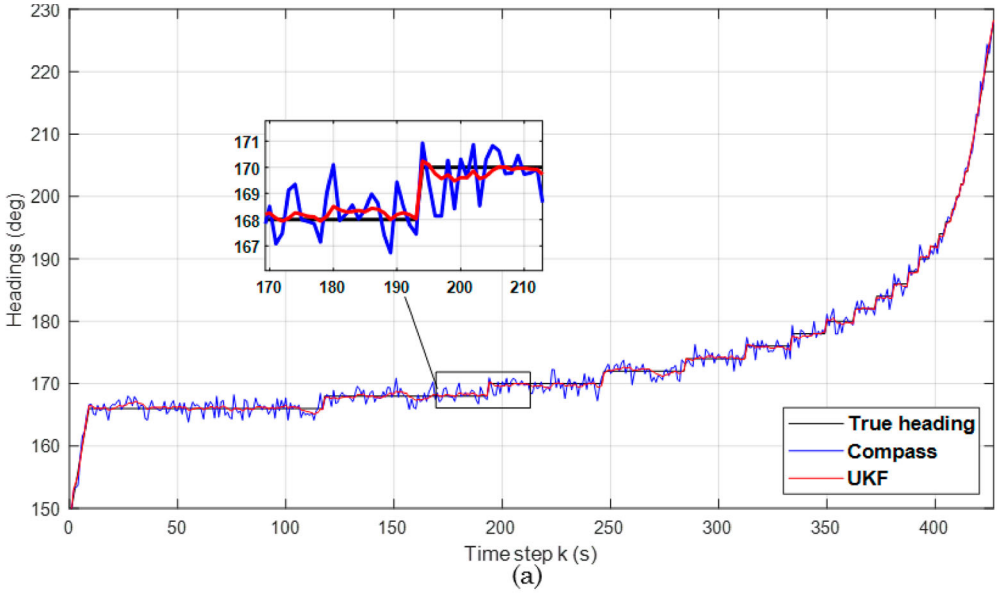

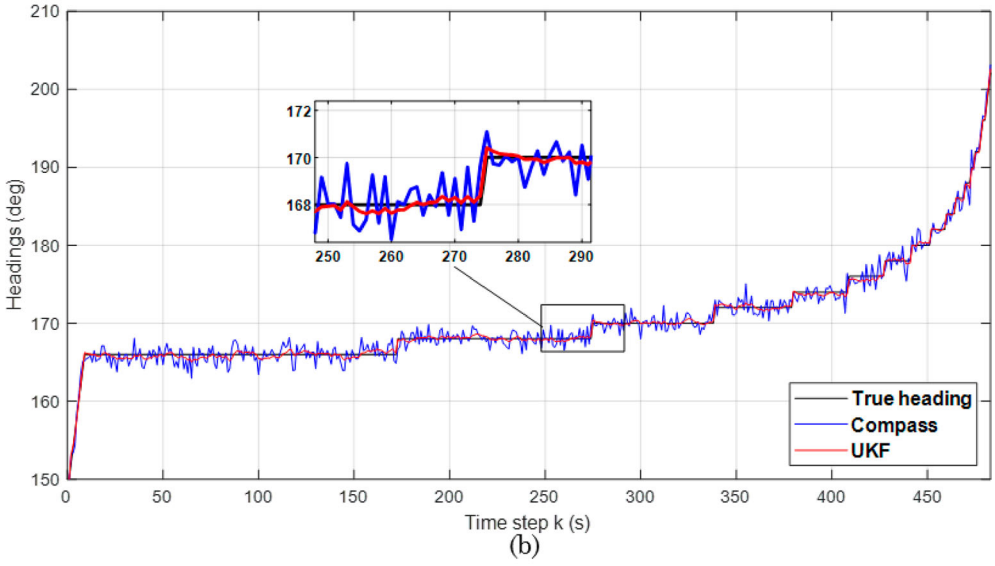

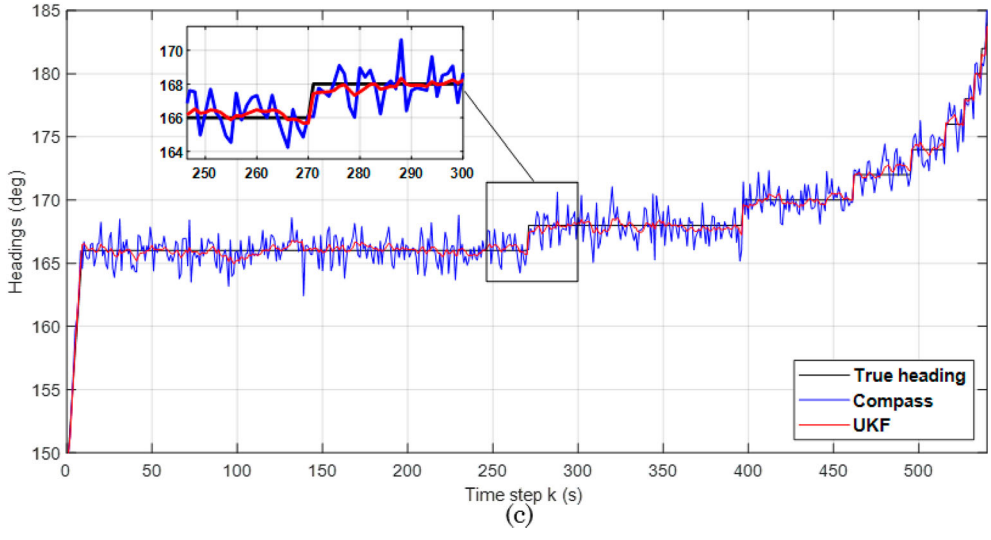

Figure 6. Simulation scenario 1: Actual headings, compass measurements and fused heading results: (a) current: 0.5 m/s; (b) current: 0.3 m/s; (c) current: 0.15 m/s.

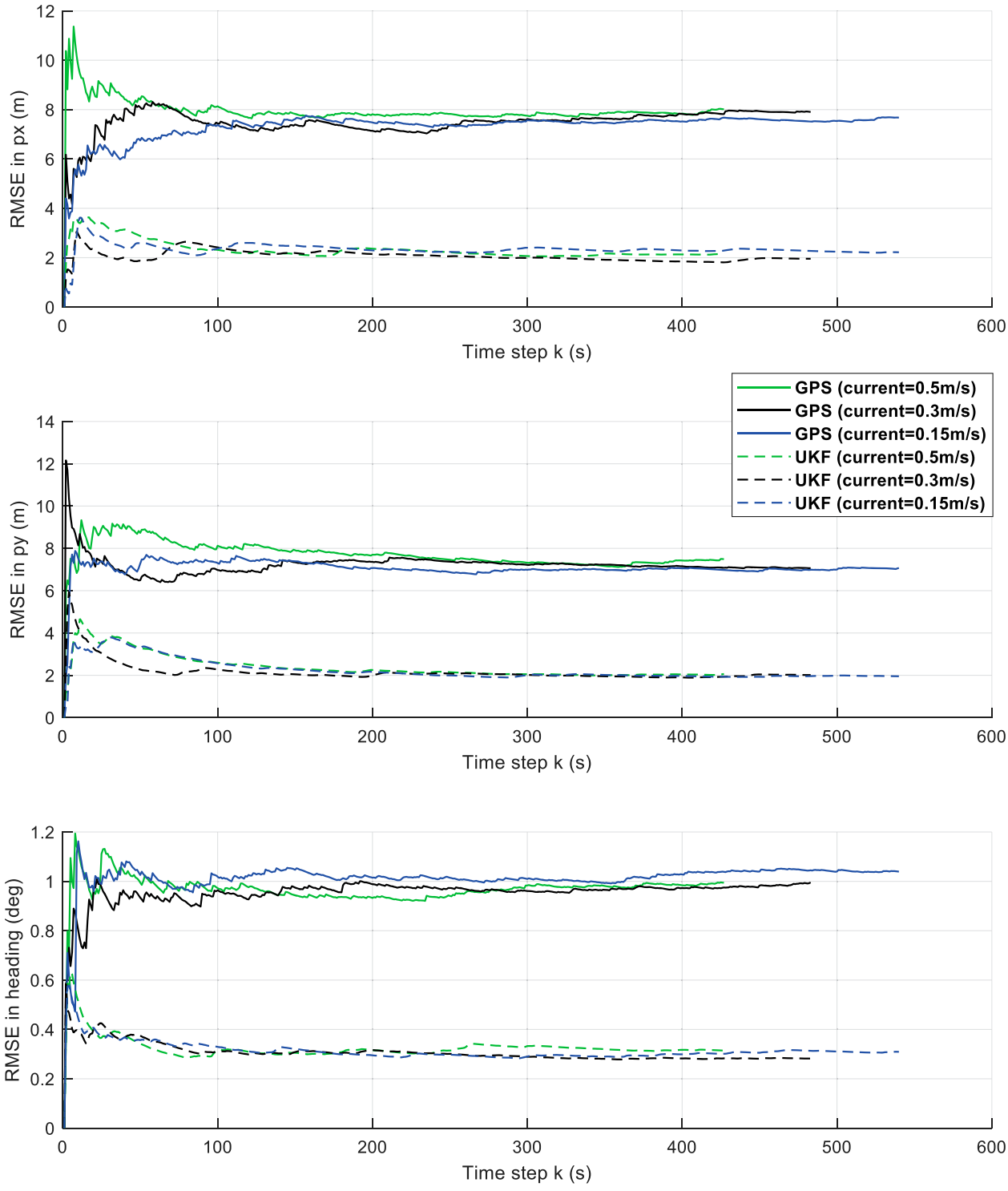

Figure 7. Simulation scenario 1: Rooted mean square errors (RMSEs) of the USV's positions and headings for the environment with three different currents.

settings are listed in Table 4 and the noisy sensor readings are simulated by generating random errors from a normal distribution with fixed mean.

5.1. Simulation scenario 1: line trajectory

The simulation area is based on the existing environment of Southampton east Cowes. Variable water currents that affect the USV's trajectory and heading are classified as an environmental disturbance. According to the environment agency, in the Southampton Water area, the tidal current at the mouth peaks at 0.7 m/s on the flood and 1.0 m/s on the ebb. The estuary flow rates are up to 0.5 m/s and up to 0.25 m/s towards the head of the rivers. The two main components of the currents are the speed and direction. In this simulation, a constant current at speed v_c along the direction of the water flows that causes drifting of the USV's position has been simulated as in Figure 3. The velocity of the USV, with respect to the shore-based reference, can then be calculated as:

$$\begin{bmatrix} v_{rx} \\ v_{ry} \end{bmatrix} = \begin{bmatrix} v_{ux} + v_c \times \cos\alpha \\ v_{uy} + v_c \times \sin\alpha \end{bmatrix} \quad (27)$$

The start and end points of the USV's trajectory are chosen to cross the water according to the satellite map as illustrated in Figure 4. The actual length of the map is 4000 m ∗ 4000 m and scaled to 800 m ∗ 800 m in this simulation. The mission of the USV is to track to the end point (517, 125 m) from the start point (365, 728 m) by following a straight line trajectory. Three simulations were conducted each with the water current in the same direction on the ebb using a different but constant speed for each simulation. The data of the currents was chosen according to the previous recorded information and tide tables for the currents in the Solent and Southampton Water. As shown in Figure 4(b), the planned straight line trajectory is altered by the influence of the water current. The blue line represents the altered trajectory by a current of 0.15 m/s. The black line (in the middle) represents the altered trajectory with a current of 0.3 m/s. The green line that shows the greatest deviation from the ideal straight line represents the trajectory altered by a current of 0.5 m/s. As would be expected the higher the velocity of the influencing current the greater the effect leading to drift from the ideal path. The initial state of the system is:

$$\boldsymbol{x}(1) = \begin{bmatrix} 365 & 728 & 0.5 & -0.866 & 150 \end{bmatrix}^T \quad (28)$$

In the simulations, the USV completed all three missions by tracking to the predesigned end points using the methodology demonstrated earlier in this section and reached the end point in the environments under the influence of three different water current speeds, 0.5, 0.3 and 0.15 m/s respectively. The trajectory results are displayed in the converted binary maps shown in Figure 5(a–c). In each figure, the actual drift affected trajectories of the USV that are represented by black lines. The simulated GPS measurements are denoted as blue dots. The red lines represent the trajectories formed by the estimated positions of the developed UKF based multi-sensor data fusion algorithm. The insets in each figure that are enlargements of part of the trajectories demonstrate the details of the simulation results. It can be seen that the red lines are very close to the black lines. The blue dots indicate that there is more noise for all three simulations, which indicates the developed UKF based multi-sensor data fusion algorithm is able to provide more accurate estimations of the USV's positions and reduce the error from the raw GPS measurements in a practical environment with water currents effects.

The estimated results of the USV headings in the environments with three different currents are illustrated in Figure 6(a–c). The effects on the USV's navigational data are more clearly shown in these three figures. When the speed of the water current is higher, the USV has to make more heading corrections to mitigate against the current influence, but it takes less time for the USV to reach the end point because the direction of the water current generally coincides USV's planned direction. Regardless of the speed of the current, it is clear that the red lines representing the fused headings closely adhere to the actual headings (black lines) with less obvious error than the compass raw measurements (blue lines) as shown in the enlarged insets.

The improved performance of the algorithm is further exemplified in Figure 7, in which the rooted mean square errors (RMSEs) of the USV's positions in the x-axis and y-axis and USV headings are demonstrated. The figure clearly shows the RMS error of the fused positions in both the x-axis and y-axis are reduced to around 2 m and the RMS error of the fused heading is reduced to less than 0.4° regardless of the water current speed. Table 5 lists the mean square errors, after the USV completes its mission that provide numerical proofs.

5.2. Simulation scenario 2: two turning manoeuvres

After proving the effectiveness of the developed UKF based multi-sensor data fusion algorithm in a simple mission with a straight line trajectory in a practical marine environment with three different constant current speeds, scenario 2 simulates a more complex environment with variable water currents and assigns manoeuvring missions to the USV instead of following a straight line. Two waypoints were set for the USV to conduct manoeuvres. The initial state is shown in Equation (29) and the planned start point, manoeuvring

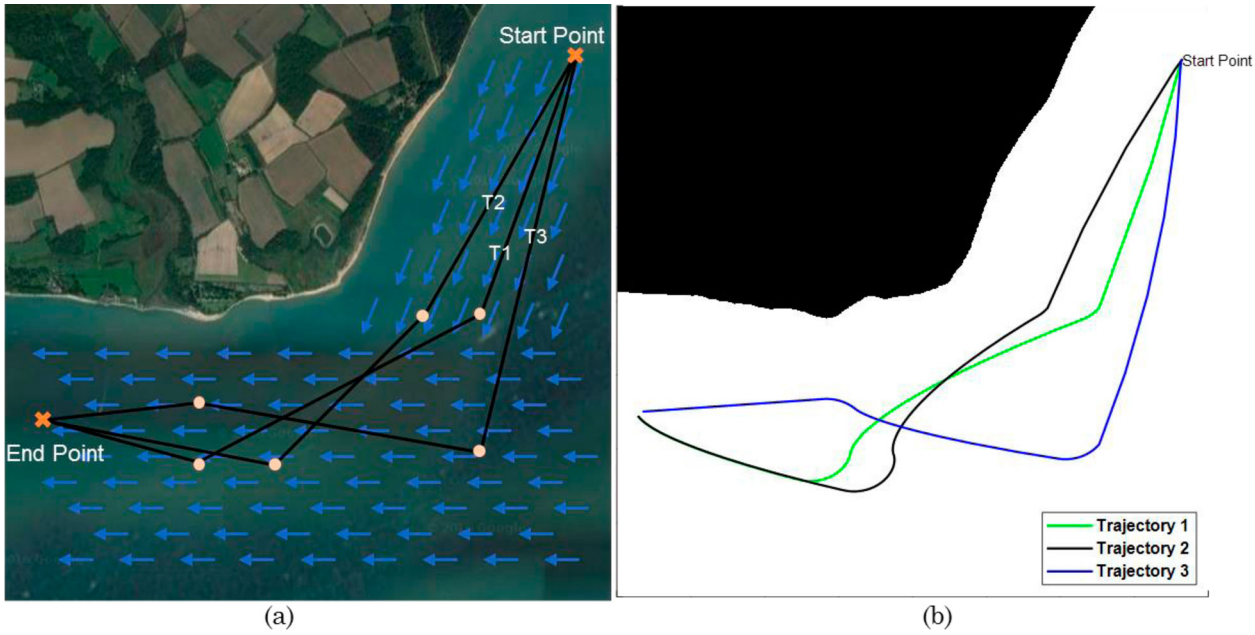

Figure 8. Simulation scenario 2: testing environment in Solent. (a) shows the satellite map with planed waypoint tracking trajectory of the USV, a varying current is simulated along the coastline; (b) gives the binary map that converted from the satellite map with the drifted trajectory of the USV caused by the varying current.

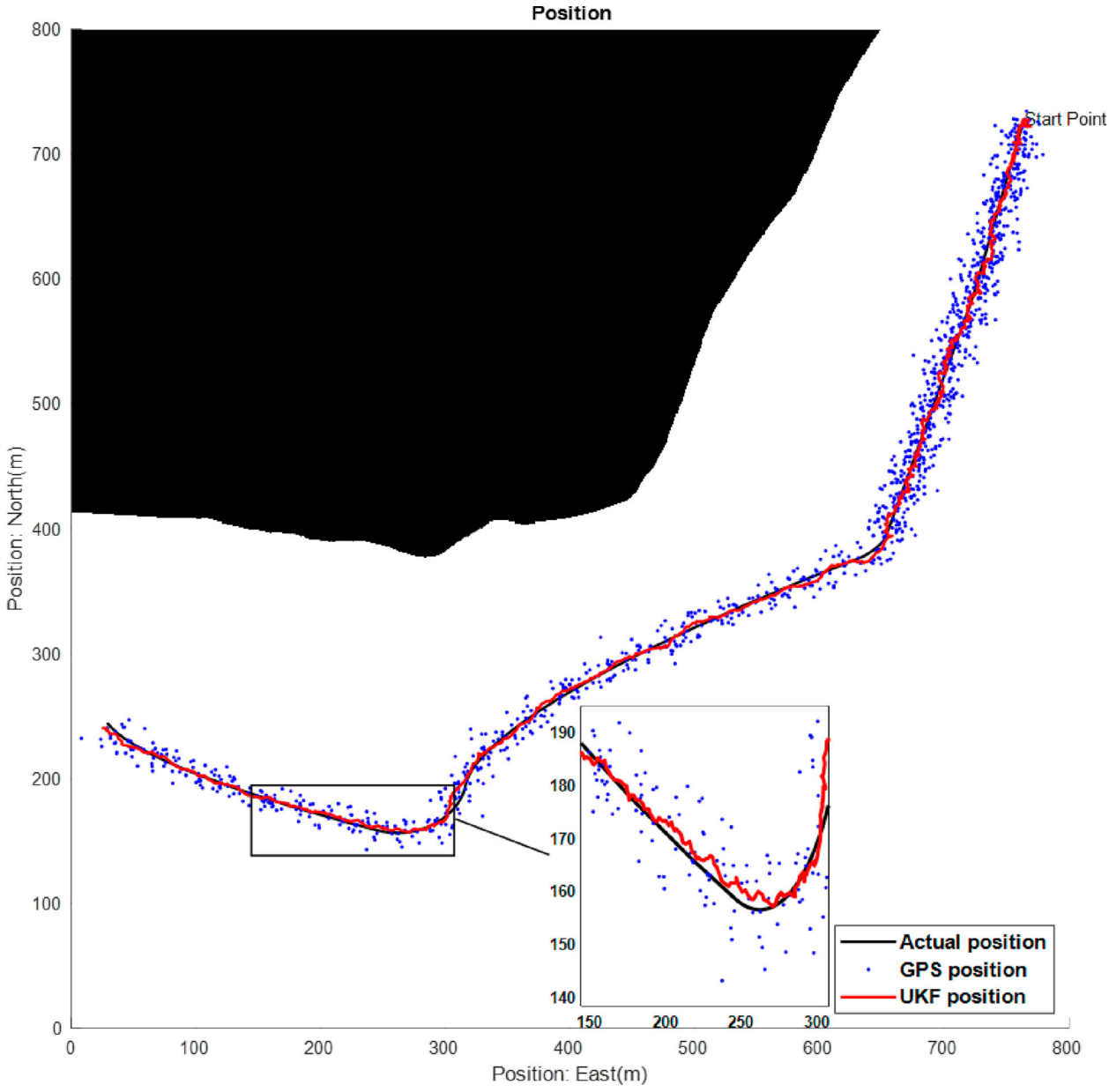

Figure 9. Simulation scenario 2: the converted binary map with the simulated GPS measurements and fused position result of planned trajectory 1.

Table 6. Waypoint settings in simulation scenario 4.4.

Planned Trajectory	Start point	Waypoint 1	Waypoint 2	End point
T1	(765,728)	(650,385)	(320,190)	(30,250)
T2	(765,728)	(580,385)	(380,190)	(30,250)
T3	(765,728)	(650,200)	(320,260)	(30,250)

waypoints and the end point are shown in Table 6.

$$\boldsymbol{x}(1) = \begin{bmatrix} 765 & 728 & -0.5 & -0.866 & 210 \end{bmatrix}^T \quad (29)$$

Figure 8(a) shows three planned manoeuvring trajectories and the water current at the speed of 0.5 m/s in varied directions. The drifted trajectories are illustrated in Figure 8(b).

Similar to the Simulation scenario 1, Figures 9–11 display the drift influenced trajectories (the black lines) of the USV for the three different missions. The GPS measurements, denoted as blue dots, are scattered around and the fused trajectories are presented as red lines. The fused trajectories are all closer to the actual trajectories regardless of the different waypoint positions. Figure 12 shows the actual headings (black line), compass measurements (blue dots) and fused headings as red lines. From the enlarged insets, it can be seen clearly that no matter where the manoeuvring waypoints are, the fused headings are much closer to the actual headings than the compass measurements. Even though the USV conducts more complicated manoeuvres in a more complex environment, the developed algorithm still performs satisfactorily in estimating the navigational data for each mission. The RMS errors and MSEs, shown in Figure 13 and Table 7, provide further evidence of the algorithm's capability in reducing raw sensor measurements for USV navigation. It can be concluded that the UKF based multi-sensor data fusion algorithm can generate good results for USV navigation in a practical environment with no restrictions on path planning.

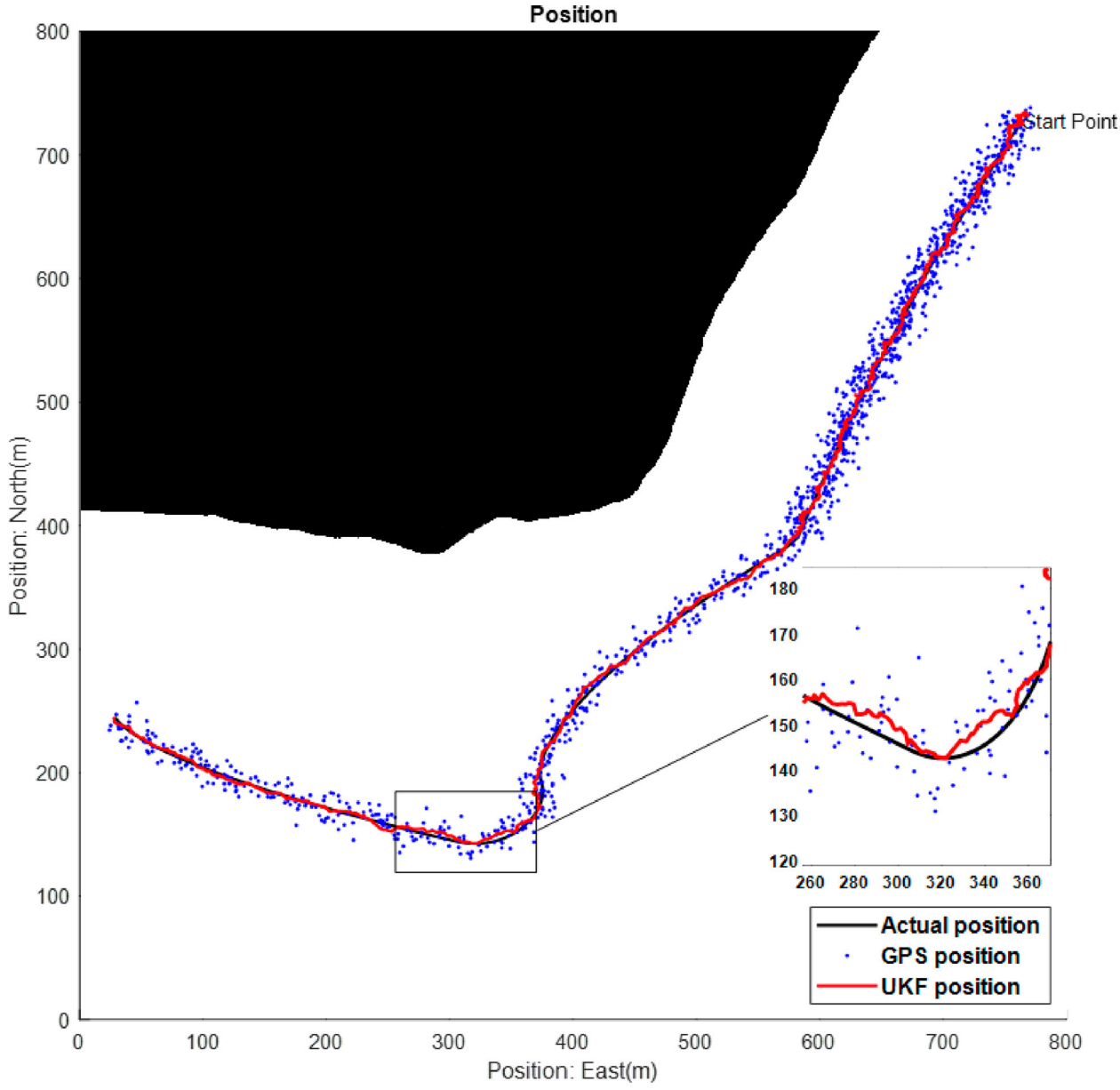

Figure 10. Simulation scenario 2: the converted binary map with the simulated GPS measurements and fused position result for planned trajectory 2.

Table 7. Simulation scenario 2: mean square errors.

Method	MSE (Tr1)	MSE (Tr2)	MSE (Tr3)	Units
UKF_position p_x	5.1926	5.7334	3.2977	m^2
UKF_position p_y	3.7565	4.8809	3.7728	m^2
GPS position p_{gpsx}	60.1971	63.1284	64.2108	m^2
GPS position p_{gpsx}	46.8124	47.041	46.8535	m^2
UKF_heading θ	0.0956	0.0863	0.0876	deg^2
Electronic Compass θ_c	0.9799	0.9473	0.9822	deg^2

6. Conclusions and future works

In this paper the effect of the inherent accuracies of navigational sensors on USV navigation was examined. Initially the use of multiple sensors to overcome such inaccuracies was proposed when it was determined that USV positional uncertainty would still exist and this uncertainty was quantified. To improve positional certainty data fusion techniques were investigated, primarily for the statically positioned USV. It was found that although the predictive-corrective iterative methodology improved positional estimation certainty, the results conversion was still affected by each particular sensors' bias and inaccuracy. To reduce the effects of the sensor noise Kalman Filtering was investigated as a means to improve the accuracy of the navigational data. A system measurement model was developed and tested by simulations with manufacturer's sensor noise performance data applied. Navigational positioning results using the UKF showed close correlation between the actual USV position and that of the predicted UKF position and improved upon the raw sensor data indication of position.

The improved accuracy of position prediction would be of great importance for motion planning and control, which are essential functions within a guidance module. For example, an improved position accuracy can assist with motion planning algorithms to generate collision-free paths with improved reliability as a USV perceives more accurately about where it starts from. In the meantime, a more accurate estimation of a USV's position during navigation

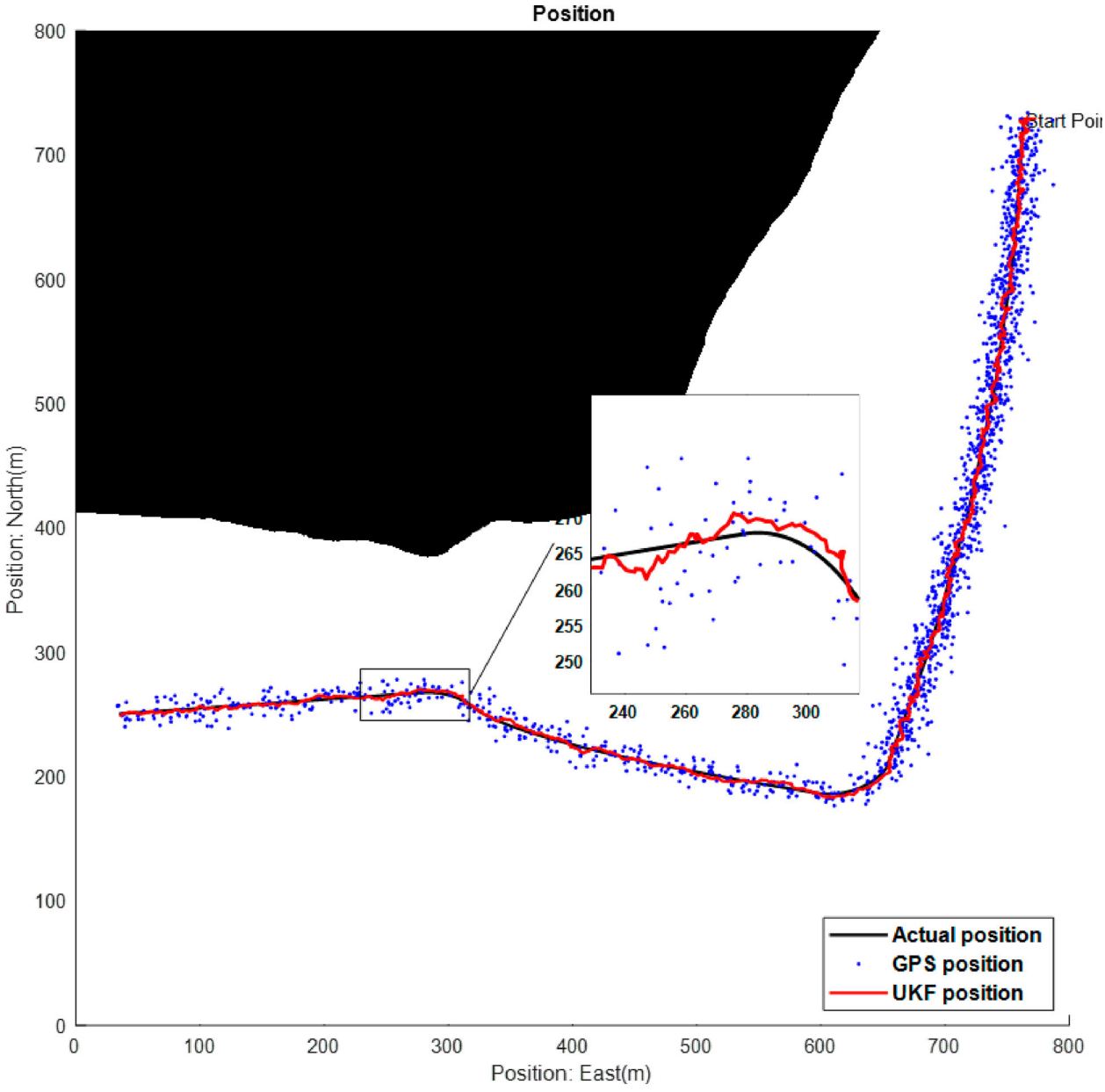

Figure 11. Simulation scenario 2: the converted binary map with the simulated GPS measurements and fused position results for planned trajectory 3.

can essentially improve the trajectory tracking performance. When a more accurate actual position information is acquired, a more precise control input can be generated by comparing it with the reference value, which as a result makes trajectory tracking (control output) more robust.

In terms of the future works, the UKF performance can be further improved by adding adaptability into the evaluation of systems and measurements covariances. This could be possibly done by integrating fuzzy logic rules when values are updated and determined. In addition, more practical evaluations, such as the real experimental tests, will need to be conducted. Work to build a new USV platform at UCL is on-going, and it is planned that a new NGC system integrated with the algorithms proposed in this paper will be developed and mounted on this USV platform for validation and verification. When it comes to practical field tests, the integration of real-time environmental data would be of importance, and these data (ocean currents, tidal currents or winds) can be expressed in the format of vector fields that have direct influences on vessels' velocities.

Looking beyond the advance of technologies, a full integration of unmanned ships into future maritime transportation requires further investigations into ships behaviours in complex practical areas. When unmanned ships are navigating together with other types of manned vessels in the same area, it is important to have a thorough understanding of different ships' collision avoidance behaviours, manoeuvring characteristics, communication strategies and navigation priorities. Given the level of complexity and difficulty associated with large-scale practical trials, it would be more promising to carry out such an investigation in a high-fidelity simulation environment. A pioneering work (Haseltalab et al. 2020) has been conducted by a collaborative research team with members from the Netherlands, Italy, Belgium and China, where a Collaborative Autonomous Shipping Experiment (CASE) was carried out to emulate future shipping environments, within which movement behaviours of different types of ships can be well simulated and studied. Also, with the advance of virtual reality (VR) and augmented reality (AR), a virtual-real simulation environment (Yang et al. 2020) with near-real environment

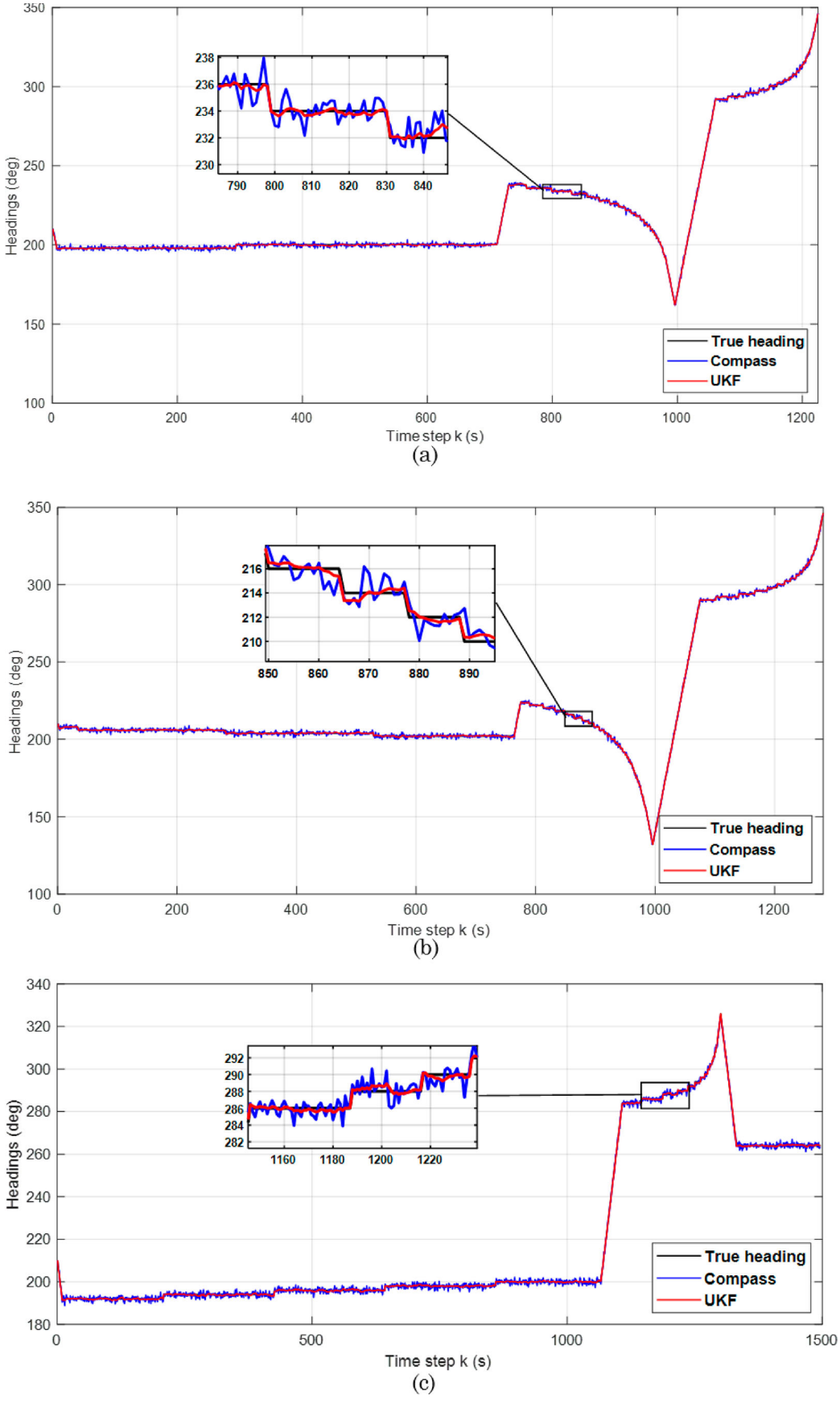

Figure 12. Simulation scenario 2: actual headings, compass measurements and fused heading results (a) planned trajectory 1; (b) planned trajectory 2; (c) planned trajectory 3.

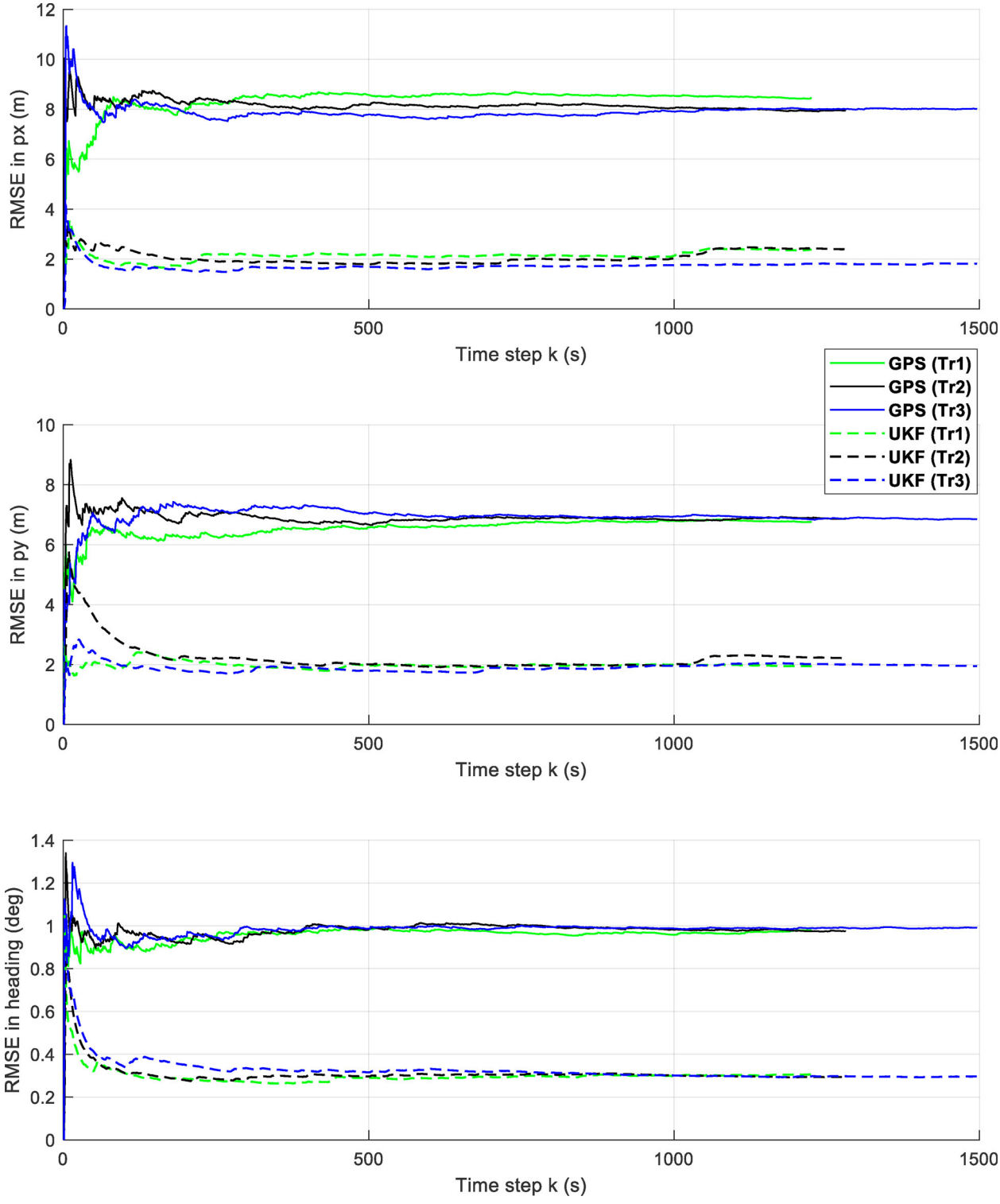

Figure 13. Simulation scenario 2: rooted mean square errors (RMSEs) of the USV's positions and headings for three different planned trajectories.

aspects can be created as a crucial testing platform to bridge the gap between pure computer-based simulations and real field trials.

Disclosure statement

No potential conflict of interest was reported by the author(s).

Notes on contributors

Wenwen Liu received the B.Eng. (H) degree in electrical and electronic engineering from Northumbria University, Newcastle upon Tyne, U.K., in 2011, the M. Sc. degree in power systems engineering and the Ph.D. degree in marine control engineering from University College London, London, U.K., in 2012 and 2020, respectively. She is currently a lecturer in Nanjing University of Technology, Information and Science, Jiangsu, China. Her research interest includes developing robust multi-sensor data fusion algorithms based on Kalman Filtering for Unmanned Surface Vehicle (USV) navigation and marine target detection.

Yuanchang Liu received the M.Sc. degree in power systems engineering and the Ph.D. degree in marine control engineering from University College London, in 2011 and 2016, respectively. He is currently a Lecturer with the Department of Mechanical Engineering, University College London. Before joining the department, he was a Research Fellow in Robotic Vision and Autonomous Vehicles with the Surrey Space Centre, University of Surrey. His research focuses on automation

and autonomy, with a special interest in the exploration of technologies for sensing and perception and guidance and control of intelligent and autonomous vehicles.

Richard Bucknall is currently a Professor of Marine Systems Engineering and the Deputy Head with the Department of Mechanical Engineering, University College London (UCL). Having gained experience working in both the shipping and rail industries as a Practicing Engineer across the world, he joined UCL as a Senior Research Associate in 1995 to follow an academic career. His research interests include electrical power systems, marine propulsion, and low-carbon technology. He has obtained research funding in excess of £10M, supervised over 25 Ph.D. students, and published over 250 articles in engineering science journals, conferences, and press.

References

Allerton DJ, Jia H. 2005. A review of multisensor fusion methodologies for aircraft navigation systems. J Navig. 58:405–417.

Appriou A. 2014. Uncertainty theories and multisensor data fusion. London and Hoboken: ISTE Ltd and John Wiley and Sons, Inc.

Baselga S, Garcia-Asenjo L, Garrigues P, Lerma JL. 2009. Inertial navigation system data filtering prior to GPS/INS integration. J Navig. 62(4):711–720.

Bijker J, Steyn W. 2008. Kalman filter configurations for a low-cost loosely integrated inertial navigation system on an airship. Control Eng Pract. 16(12):1509–1518.

Casola KJ, Beery PT, Paulo EP. 2018. System architecting and analysis of medium displacement unmanned surface vehicle "Sea hunter" as a surface warfare component of distributed lethality. Nav Eng J. 130(4):73–82.

Ccolque-Churquipa A, Cutipa-Luque JC, Aco-Cardenas DY. 2018. Implementation of a measurement system for the attitude, heading and position of a USV using IMUs and GPS. In: 2018 IEEE ANDESCON; p. 1–6.

CEE HydroSystems. 2017. CEE-USV. [accessed 2017 Mar 15]. http://www.ceehydrosystems.com/products/unmanned-survey-vessels/cee-usv/.

Chen G, Wang J, Shieh LS. 1997. Interval Kalman filtering. IEEE Trans Aerosp Electron Syst. 33(1):250–259.

Chen X, Liu Y, Achuthan K. 2021. WODIS: water obstacle detection network based on image segmentation for autonomous surface vehicles in maritime environments. IEEE Trans Instrum Meas. 70:1–13.

Choi EJ, Yoon JC, Lee BS, Park SY, Choi KH. 2010. Onboard orbit determination using GPS observations based on the unscented Kalman filter. Adv Space Res. 46:1440–1450.

Choi J, Park J, Jung J, Lee Y, Choi HT. 2020. Development of an autonomous surface vehicle and performance evaluation of autonomous navigation technologies. Int J Control Autom Syst. 18(3):535–545.

Costa RN, Pires da Silva PA, Moreira MÂ. 2019 Oct. Challenges of the design and construction of the Portuguese naval academy modular multimission unmanned surface vehicle (PoNA MM-USV. In: SNAME maritime convention. The Society of Naval Architects and Marine Engineers.

Curcio J, Leonard J, Patrikalakis A. 2005 Sept. SCOUT-a low cost autonomous surface platform for research in cooperative autonomy. In: Proceedings of OCEANS 2005 MTS/IEEE. IEEE; p. 725–729.

Gao B, Hu G, Gao S, Zhong Y, Gu C. 2018. Multi-sensor optimal data fusion for INS/GNSS/CNS integration based on unscented Kalman filter. Int J Control Autom Syst. 16(1):129–140.

Gao L, Xing J, Ma Z, Sha J, Meng X. 2012. Improved IMM algorithm for nonlinear maneuvering target tracking. Procedia Eng. 29:4117–4123.

Gelb A. 1974. Applied optimal estimation. Washington, DC: The Analytic Science Corporation.

Groves PD. 2013. Principles of GNSS, inertial, and multisensor integrated navigation systems. 2nd ed. Norwood: Artech House.

Guan G, Wang L, Geng J, Zhuang Z, Yang Q. 2021. Parametric automatic optimal design of USV hull form with respect to wave resistance and seakeeping. Ocean Eng. 235:109462.

Han J, Kim SY, Kim J. 2021. Enhanced target ship tracking with geometric parameter estimation for unmanned surface vehicles. IEEE Access. 9:39864–39872.

Han J, Xiong J, He Y, Gu F, Li D. 2017. Nonlinear modeling for a water-jet propulsion USV: an experimental study. IEEE Trans Ind Electron. 64(4):3348–3358.

Haseltalab A, Garofano V, Afzal MR, Faggioni N, Li S, Liu J, Negenborn RR. 2020. The collaborative autonomous shipping experiment (CASE): motivations, theory, infrastructure, and experimental challenges. Presented at the International Ship Control Systems Symposium (iSCSS 2020). doi:10.24868/issn.2631-8741.2020.014.

Julier SJ, Uhlmann JK. 1997 Jul. New extension of the Kalman filter to nonlinear systems. In: Signal processing, sensor fusion, and target recognition VI. Vol. 3068. International Society for Optics and Photonics; p. 182–193.

Kalman RE. 1960. A new approach to linear filtering and prediction problems. J Basic Eng. 82:35–45.

Kalman RE, Bucy RS. 1961. New results in linear filtering and prediction theory.

Langley RB. 2003. The magnetic compass and GPS. GPS World: 70–80.

Lee D, Vukovich G, Lee R. 2017. Robust unscented Kalman filter for nanosat attitude estimation. Int J Control Autom Syst. 15(5):2161–2173.

Li S, Liu J, Negenborn RR, Wu Q. 2020. Automatic docking for underactuated ships based on multi-objective nonlinear model predictive control. IEEE Access. 8:70044–70057.

Liu W, Liu Y, Bucknall R. 2019. A robust localization method for unmanned surface vehicle (USV) navigation using fuzzy adaptive Kalman filtering. IEEE Access. 7:46071–46083. doi:10.1109/ACCESS.2019.2909151.

Liu W, Liu Y, Song R, Bucknall R. 2020. Towards intelligent navigation in future autonomous surface vessels: developments, challenges and strategies. Presented at the International Naval Engineering Conference and Exhibition (iNEC 2020). doi:10.24868/issn.2515-818X.2020.052.

Li H, Pan Q, Wang X, Jiang X, Deng L. 2015. Kalman filter design for initial precision alignment of a strapdown inertial navigation system on a rocking base. J Navig. 68(1):184–195.

Liu Z, Zhang Y, Yu X, Yuan C. 2016. Unmanned surface vehicles: An overview of developments and challenges. Annu Rev Control 41:71–93.

Lv Z, Bai Y, Jin J, Wang H, Ren C. 2021. Analysis of wave fluctuation on underwater acoustic communication based USV. Appl Acoust. 175:107820.

Naeem W, Xu T, Sutton R, Tiano A. 2008. The design of a navigation, guidance, and control system for an unmanned surface vehicle for environmental monitoring. Proc Inst Mech Eng M J Eng Marit Environ. 222(2):67–79.

National Coordination Office. 2014. Official U. S. Government information about the Global Positioning system (GPS) and related topics: Marine. [accessed 2014 Nov 27]. http://www.gps.gov/applications/marine/.

Ma S, Guo W, Song R, Liu Y. 2021. Unsupervised learning based coordinated multi-task allocation for unmanned surface vehicles. Neurocomputing. 420:227–245.

Ma Y, Fang J, Wang W, Li J. 2014. Decoupled observability analyses of error states in INS/ GPS integration. J Navig. 67:473–494.

Maklouf O, Ghila A, Abdulla A, Yousef A. 2013. Low Cost IMU/GPS Integration using Kalman filtering for land vehicle navigation application. Int J Electr Comput Energet Electron Commun Eng. 7(2):184–190.

Marchel Ł, Naus K, Specht M. 2020. Optimisation of the position of navigational aids for the purposes of SLAM technology for accuracy of vessel positioning. J Navig. 73(2):282–295.

Maybeck P. 1979. Stochastic models, estimation, and control. Vol. 1. London: Academic Press, Inc.

Meng Y, Gao S, Zhong Y, Hu G, Subic A. 2016. Covariance matching based adaptive unscented Kalman filter for direct filtering in INS/GNSS integration. Acta Astronaut. 120:171–181.

Motwani A, Liu W, Sharma S, Sutton R, Bucknall R. 2016. An interval Kalman filter–based fuzzy multi-sensor fusion approach for fault-tolerant heading estimation of an autonomous surface vehicle. Proc Inst Mech Eng M J Eng Marit Environ. 230(3):491–507. doi:10.1177/1475090215596180.

Motwani A, Sharma SK, Sutton R, Culverhouse P. 2013. Interval Kalman filtering in navigation system design for an uninhabited surface vehicle. J Navig. 66:639–652.

Mousazadeh H, Jafarbiglu H, Abdolmaleki H, Omrani E, Monhaseri F, Abdollahzadeh MR, Mohammadi-Aghdam A, Kiapei A, Salmani-Zakaria Y, Makhsoos A. 2018. Developing a navigation, guidance and obstacle avoidance algorithm for an unmanned surface vehicle (USV) by algorithms fusion. Ocean Eng. 159:56–65.

Paulino ADC, Guimaraes LNF, Shiguemori EH. 2019. Hybrid adaptive computational intelligence-based multisensor data fusion applied to real-time UAV autonomous navigation. Intel Artif. 22(63):162–195.

Peng Y, Han JD, Huang QJ. 2009. Adaptive UKF based tracking control for unmanned trimaran vehicles. Int J Innov Comput Inf Control. 5(10):3505–3516.

Rodríguez M, Gómez J. 2009. Analysis of three different Kalman filter implementations for agricultural vehicle positioning. Open Agric J. 3(1).

Rødseth ØJ, Psaraftis HN, Krause S, Raakjær J, Coelho NF. 2020 Nov. AEGIS: advanced, efficient and Green intermodal systems. IOP Conf Ser: Mater Sci Eng. 929(1):012030. IOP Publishing.

Saderzadeh, A. 2010. Mobile robot navigation error handling using an extended kalman filter. J Adv Comput Res. 1(1):61–75.

Stateczny A, Kazimierski W. 2011. Multisensor tracking of marine targets–decentralized fusion of kalman and neural filters. Int J Electron Telecommun. 57(1):65–70.

Wang J, Xiao Y, Li T, Chen CP. 2020. A survey of technologies for unmanned merchant ships. IEEE Access. 8:224461–224486.

Wang N, Gao Y, Weng Y, Zheng Z, Zhao H. 2018. Implementation of an integrated navigation, guidance and control system for an unmanned surface vehicle. In: 2018 tenth international conference on advanced computational intelligence (ICACI). p. 717–722.

Wang S, Ma F, Yan X, Wu P, Liu Y. 2021. Adaptive and extendable control of unmanned surface vehicle formations using distributed deep reinforcement learning. Appl Ocean Res. 110:102590.

Xie B, Wan Y. 2011. Design of multi-sensor integrated navigation system for land vehicle. In: Multi-platform/ multi-sensor remote sensing and mapping. Xiamen: IEEE.

Yang F, Liu J, Li S, Ma F. 2020, October. Virtual-real interaction tests for functional testing of smart ships. In: The 30th International Ocean and Polar Engineering Conference; OnePetro.

Yang T, Guo Y, Zhou Y, Wei S. 2019. Joint communication and control for small underactuated USV based on mobile computing technology. IEEE Access. 7:160610–160622.

Zhai G, Meng H, Wang X. 2014. A constant speed changing rate and constant turn rate model for manoeuvring target tracking. Sensors. 14(3):5239–5253. doi:10.3390/s140305239.

Zhang P, Gu J, Milios EE, Huynh P. 2005. Navigation with IMU/GPS/digital compass with unscented Kalman filter. In: Proceedings of the IEEE International Conference on Mechatronics and Automation; July; Niagara Falls, Canada.

Zhou X, Wu P, Zhang H, Guo W, Liu Y. 2019. Learn to navigate: cooperative path planning for unmanned surface vehicles using deep reinforcement learning. IEEE Access. 7:165262–165278.

Zhou XQ, Ling LL, Ma JM, Tian HL, Yan QS, Bai GF, Liu SY, Dong L. 2015 Dec. The design and application of an unmanned surface vehicle powered by solar and wind energy. In: 2015 6th international conference on power electronics systems and applications (PESA). IEEE; p. 1–10.

Zhuang J, Zhang L, Wang B, Su Y, Sun H, Liu Y, Bucknall R. 2021. Navigating high-speed unmanned surface vehicles: system approach and validations. J Field Robot. 38(4):619–652.